Accepted Manuscript

Article submitted to: High Power Laser Science and Engineering, 2025 *January 5, 2025*

Plasma Based Prism Compressor Design for High-Intensity Laser Pulses

S. Avrutsky[1†*], J.P. Palastro[2], and A. G. R. Thomas[1*]

[1]*Gérard Mourou Center for Ultrafast Optical Science, University of Michigan, Ann Arbor, Michigan 48109, USA*

[2]*Laboratory for Laser Energetics, University of Rochester, Rochester, NY, USA*

[*]*Corresponding authors: avrut@umich.edu, agrt@umich.edu.*

[†]*Current address: Princeton University, Princeton, New Jersey 08544, USA.*

Abstract

A concept for a femtosecond pulse compressor based on underdense plasma prisms is presented. An analytical model is developed to calculate the spectral phase incurred and the expected pulse compression. A 2D particle-in-cell simulation verifies the analytical model. Simulated intensities ($\sim 10^{16}\,\mathrm{W/cm^2}$) were orders of magnitude higher than the damage threshold for conventional gratings used in chirped pulse amplification. Theoretical geometries for compact (10s cm scale) compressors for 1 PW, 10 PW, and 100 PW power levels are proposed.

1. Introduction

Since the invention of the chirped pulse amplification technique for generating high power, ultrashort pulses[1], there has been a rapid development of petawatt class facilities around the world; from one in 1998 to more than 50 in the mid-2010s[2] to several at the 10 petawatt level and beyond today[3]. There are multiple limitations to continuing to extend these facilities to ultra-high powers, but one critical technology that has been identified as a challenge[4] is the pulse compressor, which currently relies on large gratings. Conventional optics have a damage threshold that depends on the coating type and either the fluence or intensity of the incident laser light. In practice, the fluence threshold is at most 1 J/cm^2[5]. Thus, for the 0.1-1 kJ energies required to make petawatt laser pulses the gratings must be on the square meter scale or larger, which is both a technological and a cost limitation. There is, however, a scientific interest in going to further increasing the power for studies of, for example, optics in the relativistic regime[6] and beyond to the behavior of matter in extremely strong electromagnetic fields[7–9].

One alternative to conventional chirped pulse amplification using a grating compressor is the use of plasma, which has intensity limits for degradation of performance that are many orders of magnitude higher than conventional optical elements. In principle, plasma could be used to compress a chirped pulse through group velocity dispersion, which recently has been theoretically demonstrated for mm-scale, near critical-density plasma[10]. At lower plasma densities, however, the required path lengths would be too long for practical use. This motivates the use of a structured plasma which can take advantage of geometric dispersion to compress a pulse over a much smaller region of space (or with a much smaller spatial footprint).

The use of parametric processes, such as Raman[11,12] and Brillouin[13,14] scattering has been explored for amplifiers or for volume compression using plasma Bragg gratings[15]. These schemes rely on the generation of periodic structures and operation at near-relativistic laser intensities, $I\lambda^2 \gtrsim 10^{17}\ \mathrm{W/cm^2}$, where I is the intensity and λ is the wavelength. At such intensities there are multiple nonlinear processes that can degrade performance, e.g. wavebreaking and pre-depletion of the pump laser pulses by thermal plasma[16], and laser filamentation instabilities[17]. More recent studies have considered the replacement of the conventional gratings with transient plasma transmission gratings [18,19]. As transmission gratings require a small amount of plasma and the dispersion comes from geometric considerations the scheme should be less sensitive to nonlinearities or plasma inhomogeneity. Another method for obtaining the required angular dispersion is through transverse plasma density gradients, which have previously been studied in the context of plasma lenses[20–22] and for laser steering[23,24].

In this paper, we present an approach for pulse compression using prisms of uniform underdense plasma that may be made using shaped gas cells, as shown in Figure 1.

10.1017/hpl.2025.18

https://doi.org/10.1017/hpl.2025.18 Published online by Cambridge University Press

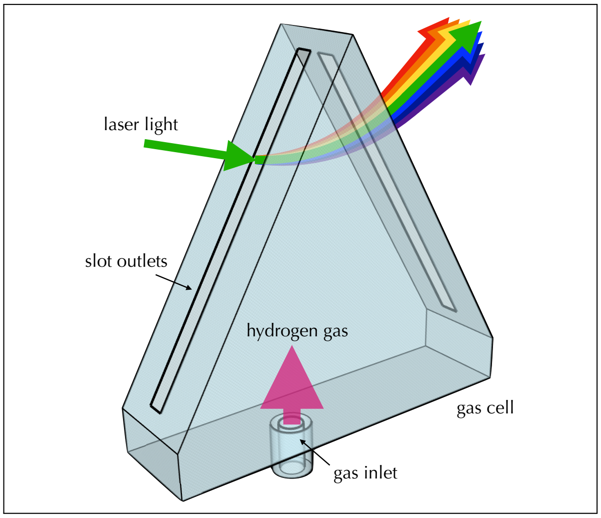

Figure 1. Schematic of a plasma prism based on ionization of hydrogen gas in an additively manufactured gas cell[25].

This design has the advantages of beginning only with gas (and so reproducible at high repetition-rate), using simple geometry, withstanding intensities several orders of magnitude higher than conventional gratings, and remaining relatively compact. With these advantages, plasma-prism compression may offer an approach to plasma-based compression for the next generation of high-power lasers.

2. Dispersion in plasma

The linear dispersion relation for light propagating in an unmagnetized plasma is $\omega^2 = c^2k^2 + \omega_p^2$, where $\omega_p = \sqrt{e^2 n_e/m_e\varepsilon_0}$ is the plasma frequency for electron number density n_e. The refractive index is therefore $n(\omega) = \sqrt{1-\omega_p^2/\omega^2}$. For convenience, we define the relative density of plasma $N = n_e/n_c$, where $n_c = \varepsilon_0 m_e \omega_0^2/e^2$ is the critical density for the central frequency of the laser, ω_0, and ε_0, e, and m_e are the vacuum permittivity and electron charge and mass.

The temporal profile of a linearly-chirped Gaussian pulse can be expressed as

$$E(t) = E_0 \Re\{e^{-i\omega_0 t} e^{-\frac{1}{2}(1+iC_0)(t/\tau_0)^2}\} \tag{1}$$

where E_0 is the pulse amplitude, τ_0 is the half-width at $1/e$ level of intensity, and C_0 is the linear chirp factor. The bandwidth-limited duration of the pulse is $\tau_1 = \tau_0/\sqrt{1+C_0^2}$. The frequency bandwidth of the pulse may be quantified by the half width of $|\hat{E}(\omega)|^2$ at 1/e level, $\Delta\omega = 1/\tau_1$[26].

A frequency component ω propagating in a dispersive medium will incur a spectral phase $\Psi(\omega) = \omega P/c$, where P is the optical path length,

$$P = \int n(\vec{r})dr \tag{2}$$

integrated along the frequency-dependent path of propagation. Expanding Ψ in a Taylor series about ω_0 yields

$$\begin{aligned}\Psi = \Psi_0 + (\omega-\omega_0)\Psi_0' + \frac{1}{2}(\omega-\omega_0)^2\Psi_0'' \\ + \frac{1}{6}(\omega-\omega_0)^3\Psi_0''' + \dots\end{aligned} \tag{3}$$

where $\Psi_0 = \Psi(\omega_0)$ and $\Psi_0' = \partial\Psi/\partial\omega|_{\omega=\omega_0}$ are the phase and group delays, respectively, which only displace the pulse but do not affect the phase fronts or temporal profile. The second order phase

$$\Psi_0'' \equiv \left.\frac{\partial^2\Psi}{\partial\omega^2}\right|_{\omega_0} = \frac{1}{c}\left.\left(2\frac{\partial P}{\partial\omega} + \omega\frac{\partial^2 P}{\partial\omega^2}\right)\right|_{\omega_0} \tag{4}$$

is the Group Delay Dispersion (GDD) incurred within the medium.

Depending on its sign, the GDD will increase or decrease the linear chirp of a pulse. For instance, the GDD necessary to compress a linearly chirped pulse to the bandwidth limit is $\Psi_0'' = C_0\tau_0^2/(1+C_0^2)$[26]. Third Order Dispersion (TOD),

$$\Psi_0''' \equiv \left.\frac{\partial^3\Psi}{\partial\omega^3}\right|_{\omega_0} = \frac{1}{c}\left.\left(3\frac{\partial^2 P}{\partial\omega^2} + \omega\frac{\partial^3 P}{\partial\omega^3}\right)\right|_{\omega_0} \tag{5}$$

and higher order terms will distort the Gaussian pulse shape. The spectral phase incurred within an optical system will affect a pulse traveling through it via $E_{post}(\omega) = E_{pre}(\omega)e^{i\Psi(\omega)}$.

3. Compressor Design

The prism compressor is constructed from four plasma prisms. Figure 1 shows a concept for implementation of such a plasma prism in practice, based on additively manufactured gas cells that have been used successfully in laser-wakefield acceleration experiments[25]. The prisms are arranged symmetrically across a central "mirror" axis, as shown in Figure 2. The apexes of the prisms are spaced a distance L apart with the second prism apex elevated above the first, forming an angle α. The mirror axis is at a distance M from the tip of the second prism. Each prism has a uniform relative plasma density $N < 1$. All frequency components enter the first prism and exit the second prism at Brewster's angle $\theta_B = \arctan\left(\sqrt{1-N}\right)$ with respect to the surface. The half-angle of each prism is Brewster's angle in plasma $\theta_B' = \arctan\left(1/\sqrt{1-N}\right)$. A ray with frequency ω enters the second prism at an angle φ_2, which becomes φ_2' inside the prism. On the other boundary, it exits the plasma at angle φ_1', which becomes θ_B upon exit to vacuum. These angles can be expressed in terms of the frequency and refractive index of the plasmas as follows:

$$\varphi_2(\omega) = \arcsin\left(\sin 2\theta_B' \cdot \sqrt{n^2(\omega) - \sin^2\theta_B} - \cos 2\theta_B' \cdot \sin\theta_B\right) \tag{6}$$

$$\varphi_2'(\omega) = 2\theta_B' - \varphi_1'(\omega) \tag{7}$$

$$\varphi_1'(\omega) = \arcsin\left(\sin\theta_B / n(\omega)\right) \tag{8}$$

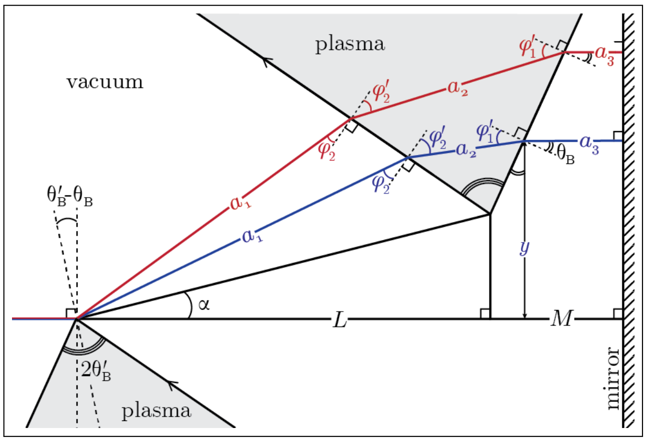

Figure 2. Path of lower frequency (red) and higher frequency (blue) rays through the plasma prism compressor.

A ray with frequency ω which travels through the tip of the first prism will travel a length a_1 between the two prisms, a_2 within the second prism, and a_3 from the second prism to the mirror. Lengths $a_1, a_2,$ and a_3 are a function of frequency and are derived from the geometry of the prism arrangement as follows:

$$a_1 = \frac{L}{\cos\alpha}\frac{\cos(\alpha+\theta_B-2\theta_B')}{\cos\varphi_2} \tag{9}$$

$$a_2 = \frac{L}{\cos\alpha}\frac{\sin 2\theta_B' \sin(2\theta_B'-\theta_B-\alpha-\varphi_2)}{\cos\varphi_2\cos\varphi_1'} \tag{10}$$

$$a_3 = M - \frac{L}{\cos\alpha}\frac{\sin\theta_B\cos\varphi_2'\sin(2\theta_B'-\theta_B-\alpha-\varphi_2)}{\cos\varphi_2\cos\varphi_1'} \tag{11}$$

Assuming sharp vacuum-plasma boundaries, the integration in Eqn. 2 can be estimated as $P(\omega) = 2[a_1(\omega) + n(\omega)a_2(\omega) + a_3(\omega)]$. In principle, it is not necessary for the boundaries to be sharp for the concept to work, since for refraction under the ray-tracing approximation Snell's law holds for non-sharp transitions, but it simplifies the calculations. In practice, the additional phase accumulation from boundary ramps could be pre-compensated using a spectral phase control device.

The overall spectral phase applied by the compressor is parameterized by N, L, and α, i.e. $\Psi = \Psi(\omega; N, L, \alpha)$. The compressor geometry was optimized using these parameters such that $\Psi_0'' = C_0\tau_0^2/(1+C_0^2)$ and higher order distortions were minimized. To quantify the distorting effect of TOD in particular, the parameter $q = \frac{1}{6}\Psi_0'''\Delta\omega^3$ is defined as the contribution of TOD to the incurred phase at $\omega = \omega_0 + \Delta\omega$.

Figure 3 shows the parameter phasespace of L and α such that $\Psi_0'' = 10000$ (e.g., designed to compress a pulse with $\tau_0 = 1000$, $C_0 = 100$ fs to $\tau_1 = 10$ fs) for normalized densities N varying from 0.1 to 0.005 and assuming sharp plasma boundaries. The angle α is defined to be negative

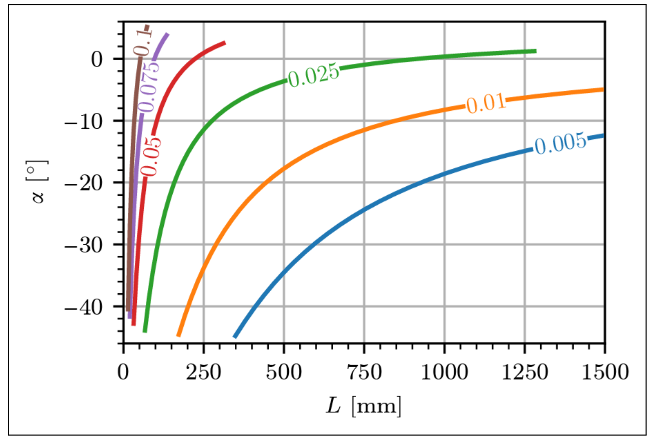

Figure 3. Allowed values of L and α such that $\Psi_0'' = 10000$ for densities N varying from 0.1 to 0.005 (colored lines, labeled).

when the apex of the second prism is below the first, and is limited above by the angle of refraction of the highest frequency in the pulse and limited below by the first prism. Thus α is constrained by $\Psi_0''(\omega_{max}) < 2\theta_B' - \theta_B - \alpha < \pi/2$, where ω_{max} can be approximated as $\omega_0 + 2\Delta\omega$. Larger densities and more negative values α apply the necessary GDD in less distance. While the initial linear chirp is eliminated from the pulse, TOD is significant in this region of parameter space. Using Eqns 9-11 and 5, we calculate q along each line plotted in Figure 3 and plot it in Figure 4. q decreases with decreasing N and decreasing α, but always remains $q > 2$. The criteria for minimal shape distortion is $q \ll 0.1$, which is not possible by optimizing parameters N, L, and α alone.

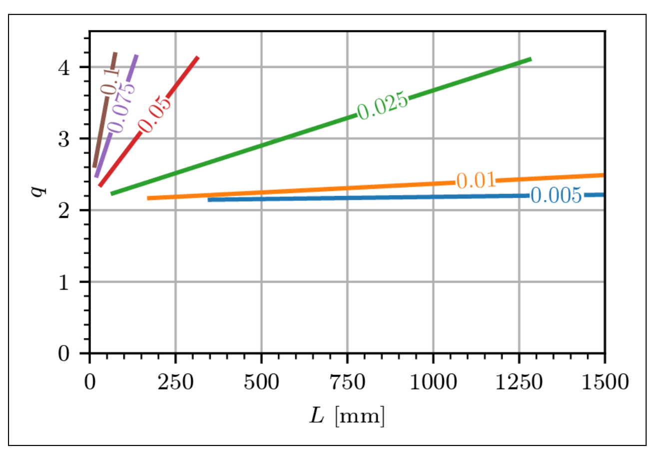

Figure 4. Third-order distortion q for densities N varying from 0.1 to 0.005 such that $\Psi_0'' = 10000$ showing that TOD needs compensation for.

https://doi.org/10.1017/hpl.2025.18 Published online by Cambridge University Press

Figure 5 shows the shape distorting effects of TOD on a bandwidth-limited pulse. When q is 0, the pulse is near transform-limited. As $|q|$ increases, the peak intensity drops, and additional peaks appear earlier in time.

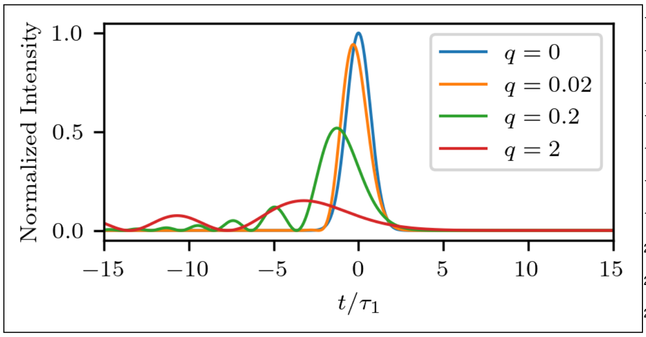

Figure 5. Effects of third order dispersion on a bandwidth-limited pulse showing that $q > 2$ corresponds to a severe TOD phase error.

3.1. *Third order dispersion correction*

To correct third order dispersion errors, the spectral phase of the uncompressed pulse may be pre-compensated in the front end of the laser chain. Alternatively, a correcting plasma slab with a polynomial density profile can be inserted at the mirror axis to compensate for the TOD. This is the position where the frequency components of the incoming pulse are spatially dispersed, vertically.

Halfway through the compressor, a ray with frequency ω is located a distance y above the first prism:

$$y(\omega) = \frac{L}{\cos\alpha}\left[\sin\alpha + \frac{\cos\theta_B \cos\varphi_2' \sin(2\theta_B' - \theta_B - \alpha - \varphi_2)}{\cos\varphi_1' \cos\varphi_2}\right] \quad (12)$$

which to first order in frequency is $y(\omega) = y_0 + A(\omega - \omega_0)$. Define a rectangular slab of plasma centered horizontally at the mirror axis with width W and relative density profile $N(y(\omega)) = N_0 + B(y - y_0)^3$. The spectral phase accumulated over a length W is

$$\Psi(\omega) = \frac{\omega}{c} W n(\omega) = \frac{\omega}{c} W \sqrt{1 - \frac{N(\omega)\omega_0^2}{\omega^2}} \quad (13)$$

for which the GDD is

$$\left.\frac{\partial^2\Psi}{\partial\omega^2}\right|_{\omega_0} = \frac{W}{c\omega_0\sqrt{1-N_0}}\left(\frac{N_0}{1-N_0}\right), \quad (14)$$

and the TOD is

$$\left.\frac{\partial^3\Psi}{\partial\omega^3}\right|_{\omega_0} = \frac{-3W}{c\omega_0^2\sqrt{1-N_0}}\left(\frac{N_0}{(1-N_0)^2} - BA^3\omega_0^3\right). \quad (15)$$

From Eqn. 5 and Eqn. 15, it follows that B must equal

$$B = \frac{1}{A^3\omega_0^3}\left(\frac{N_0}{(1-N_0)^2} + \Psi_0''' \frac{c\omega_0^2}{3W}\sqrt{1-N_0}\right) \quad (16)$$

and the correcting slab will compensate for the TOD incurred by the other four prisms.

4. Simulation in OSIRIS

The full plasma-prism compressor, including TOD compensation, was simulated in 2D with the particle-in-cell framework OSIRIS[27,28]. OSIRIS solves Faraday and Ampere's laws in differential form using the finite-different-time domain technique. By solving these equations, OSIRIS captures effects that cannot be modelled with raytracing, such as the finite pulse width and duration and nonlinear plasma dynamics.

The laser pulse is initialized with a Gaussian temporal and transverse profile with $1/e$ intensity duration τ and width w_0. The pulse in vacuum and the simulation window move in the x direction at the speed of light. The window was $4000\ c/\omega_0 \times 4500\ c/\omega_0 = 509\,\mu\text{m} \times 573\,\mu\text{m}$ in size and had $8192 \times 8192 = 6.7 \times 10^7$ grid points. The time step used was $\Delta t = 0.395/\omega_0 = 0.168\,\text{fs}$. Each simulation cell contained 2 electrons, for a total of 1.3×10^8 particles. For a pulse wavelength of $0.8\,\mu\text{m}$, the (angular) frequency is $\omega_0 = 2.355\ \text{fs}^{-1}$. The laser pulse started with length $\tau_0 = 100$ fs, chirp factor $C_0 = 10$, amplitude $a_0 = 0.05$, and spot size $w_0 = 12.84\ \mu\text{m}$, corresponding to a Rayleigh length of $z_R = 647\ \mu\text{m}$. $a_0 = eE_0/(m_e c\omega_0)$ is the normalized vector potential amplitude of the laser electric field. The pulse was polarized in the x-y plane. The prism system had relative plasma density $N = 0.2$, distance between apexes $L = 800$ µm, and angle $\alpha = -8°$. The correction slab had width $W = 100\,\mu\text{m}$, central relative density $N_0 = 0.03$, and density growth factor $B = 1.512 \times 10^{-7}\ \mu\text{m}^{-3}$.

Figure 6 shows the intensity profile of the pulse overlaid on the prism compressor at seven locations along its trajectory. Simulation outputs are plotted roughly every 1.8 ps. The pulse can be seen compressing in duration as it it travels from left to right through the system. The system is symmetric about the mirror axis at $x = 1350\ \mu\text{m}$. The dashed lines show the results of ray tracing through the compressor for frequencies $\omega_0 \pm 2\Delta\omega$, calculated by applying Snell's law at each boundary and propagating to the next boundary. The simulated pulse remains confined by these paths for roughly three Rayleigh lengths before the effects of diffraction can be observed in the transverse spreading of the pulse. This spreading could be mitigated by beginning with a larger spot size $w_0 \geq 2\sqrt{c(L+M)/\omega_0}$, such that the length of the system is no more than one Rayleigh length.

Figure 7 compares the initial and final pulse profiles with the transform-limited profile and theoretically predicted profile. The simulated pulse ends with a full width at half-maximum (FWHM) of 22.4 fs, a compression ratio of 7.4 from its initial duration of 166.5 fs and 1.3 times the transform-limited duration of 16.6 fs. The simulated profile has a 20% narrower FWHM and longer tails than the analytical profile, likely due to wavefront curvature that the

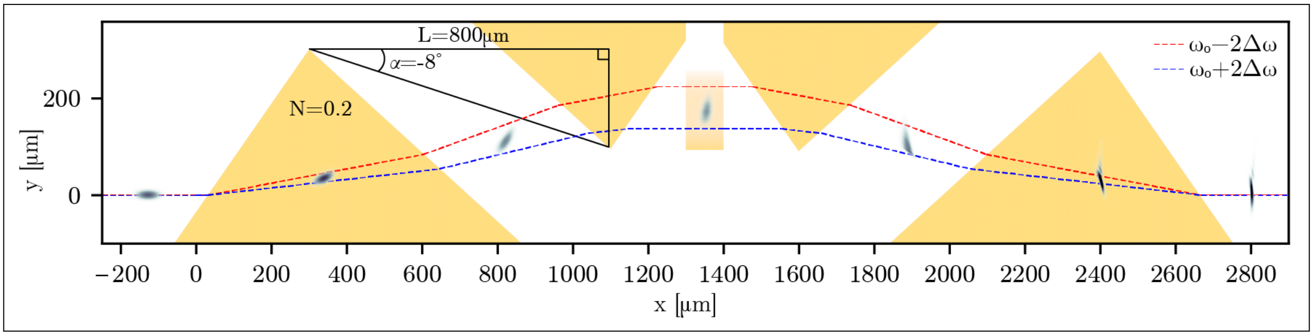

Figure 6. Full compression of a pulse with duration $\tau_0 = 100$ fs is simulated in Osiris using a plasma prism system. The plasma density profile is plotted in yellow. Seven simulation outputs are plotted with timestamps. The dashed lines show the expected paths of $\omega_0 \pm 2\Delta\omega$ frequency components.

theory cannot account for. Both have a peak power of 83 GW.

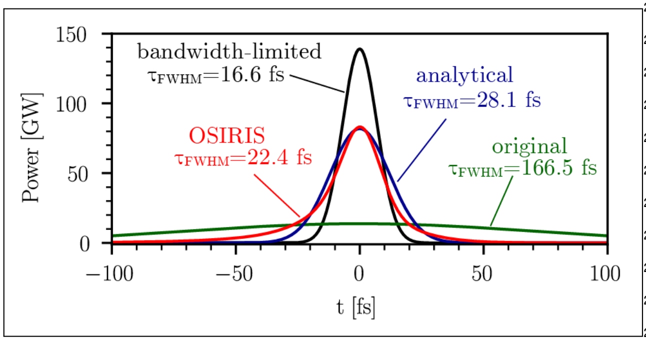

Figure 7. Comparison of initial, simulated, analytical, and transform-limited pulse power profiles.

5. Discussion

The Osiris simulation confirms the feasibility of femtosecond pulse compression using plasma prisms. Estimating the resulting pulse shape given a particular compressor geometry with the analytically derived expressions can be completed near instantly, whereas the Osiris simulation ran in parallel for roughly 12 hours on 36 cores. The compressor used a relatively high density of $N = 0.2$ to shrink the system to less than 3 mm in length to reduce computation time. There are other effects which need to be accounted for to improve the accuracy of this analytical estimation, including diffraction, wavefront curvature, and more realistic density profiles at the prism-vacuum interfaces. However, it should be noted that, having been successfully demonstrated by direct ab-initio simulation at high density/compact size, scaling up to higher powers with larger focal spots, where the Rayleigh length is longer, would be even more accurately described by the ray-tracing.

The compression of a pulse is sensitive to the exact GDD incurred. The simulation geometry applies a GDD of $864\,\mathrm{fs}^2$, 13.6% less than the $1000\,\mathrm{fs}^2$ necessary to achieve the transform limit. The resulting pulse is 35% longer and has 38% less power than if it were transform-limited. The system geometry could be further optimized to compress pulses closer to the bandwidth-limit.

Additional Osiris simulations (not shown) indicate that the trajectory of the pulse remains largely unaffected when the sharp plasma boundaries are replaced by 200 μm ramps. However, the GDD is sensitive to the presence of the ramp (because of the added optical path). To incorporate this into the analytical expressions one would need to trace the frequency-dependent trajectory in a density gradient and integrate the optical path length in Eqn. 2. Step-function boundaries were assumed in the derivation of Eqns 9-11 so that closed-form expressions for the partial derivatives in Eqns 4 and 5 would exist.

In the case of femtosecond pulses, the damage threshold for conventional diffraction gratings is on the order of 10^{13}-10^{14} W/cm^2 [29,30]. The peak intensity of the simulated pulse reached 1.14×10^{16} W/cm^2. At this intensity, no nonlinear phenomena that could disrupt the compression process were observed. Though the simulated pulse power reached 83 GW, self-focusing was not observed. The critical power for self-focusing is $P_{cr} \approx (17/N)$ GW [31], which for the parameters here means that $P/P_{cr} \sim 1$. Even for higher powers, however, previous studies have shown that self-focusing may not occur for ultra-short pulses even if the pulse peak power is many times larger than the critical power [32,33].

The fastest growing parametric instability that can disrupt the compression would be stimulated Raman scattering (SRS). A positive chirp in ultra-short pulses in underdense plasma has been found to increase backward SRS [34,35]. Limiting backward SRS by constraining $\gamma_0 \tau_{FWHM} < 12$, where $\gamma_0 = (1/2) a_0 \omega_0 \sqrt{(\omega_p/\omega_0)/(1-\omega_p/\omega_0)}$ is the SRS growth rate [36], imposes an upper bound on the peak laser intensity and optimal system geometry. In terms of the prism density N, this constraint can be expressed as $N < 1/(1 + (\ln 2/144)(\omega_0 a_0 \tau_0)^2)^2$. For the simulated parameters $N = 0.2$ is less than $N_{SRS} = 0.36$, which is consistent with the absence of SRS in the simulations.

Given the constraints on beam spot size and prism density, Table 1 lists theoretical design parameters that could be

https://doi.org/10.1017/hpl.2025.18 Published online by Cambridge University Press

	1 PW	10 PW	100 PW
a_0	0.01	0.01	0.01
w_0 [mm]	1.7	5.5	17
N	0.05	0.03	0.01
α [°]	-6	-16	-24
L [mm]	131	151	364
M [mm]	100	100	140
N_0	0.01	0.01	0.01
W [mm]	10	10	10
B [mm^{-3}]	3.79×10^{-4}	9.70×10^{-4}	1.75×10^{-3}

Table 1. Proposed design parameters for higher power compressors that supply a GDD of 1000 fs^2.

used for compact high power systems that incur a GDD of 1000 fs^2, such as for compressing a $\tau_0 = 1$ ps, $C_0 = 100$ pulse to $\tau_1 = 10$ fs. The total system size for these compressors is on the scale of 1 meter. Note that in practice, the gas would require ionization. For hydrogen gas the barrier suppression ionization (BSI) intensity is of order 10^{14} W/cm^{-2}, which is two orders of magnitude below the peak intensity and so the gas may be considered to be fully ionized far before the main pulse peak intensity. However, the initial 1 ps long chirped pulse would be close to the BSI intensity and may therefore require some system for (pre-)ionizing the plasma along the laser path, e.g., ionization by a second laser, electrical discharge or cylindrically focusing in the z direction to result in higher intensity in the earlier prisms.

6. Conclusion

Ionization of the plasma will be an important consideration for an experimental demonstration. It should also be noted that the studies here only considered only collisionless ideal plasma, but it is clear that thermal corrections, fluctuations, collisional effects, etc. will affect the dispersive properties of the plasma prisms and potentially laser energy absorption. For random fluctuations, however, the resulting phase errors may be expected to average to zero over long scales. The effects of ionization and neutral gas as well as non-sharp plasma-vacuum boundaries may generate non-zero averaging phase errors that may need compensation. Proof-of-principle experiments and detailed calculations investigating these effects are left for further work.

A novel compressor for high-power femtosecond pulses based on underdense plasma prisms, can operate at intensities that are orders of magnitude higher than systems using diffraction gratings or solid-state prisms. An analytical model was developed to calculate the spectral phase acquired in the compressor and the corresponding pulse compression. The theory was verified with OSIRIS PIC simulations. Using only plasma prisms, it is impossible to completely eliminate TOD through geometric optimization. However, the TOD could be compensated in laser front end or by introducing a plasma slab with a cubic density profile at the center of the compressor. Within these constrains, a compact high-power compressor with overall dimensions less than 1 meter can be designed. At the intensities simulated (10^{16} W/cm^2), neither self-focusing nor stimulated Raman scattering were observed.

7. Acknowledgments

This work was supported by US NSF awards 2108075 and 2126181. The work of JPP was supported by the Office of Fusion Energy Sciences under Award Number DE-SC0021057, the Department of Energy National Nuclear Security Administration under Award Number DE-NA0004144, and the New York State Energy Research and Development Authority. This research was supported in part through computational resources and services provided by Advanced Research Computing at the University of Michigan, Ann Arbor.

References

1. Donna Strickland and Gerard Mourou. Compression of amplified chirped optical pulses. *Optics Communications*, 56:219, 1985.
2. Colin Danson, David Hillier, Nicholas Hopps, and David Neely. Petawatt class lasers worldwide. *High Power Laser Science and Engineering*, 3:e3, 2015.
3. Colin N. Danson, Constantin Haefner, Jake Bromage, Thomas Butcher, Jean-Christophe F. Chanteloup, Enam A. Chowdhury, Almantas Galvanauskas, Leonida A. Gizzi, Joachim Hein, David I. Hillier, and et al. Petawatt and exawatt class lasers worldwide. *High Power Laser Science and Engineering*, 7:e54, 2019.
4. Engineering National Academies of Sciences and Medicine. *Opportunities in Intense Ultrafast Lasers: Reaching for the Brightest Light*. The National Academies Press, Washington, DC, 2018.
5. Wenfei Zhang, Weijin Kong, Guomei Wang, Fei Xing, Fang Zhang, Huanian Zhang, and Shenggui Fu. Review of pulse compression gratings for chirped pulse amplification system. *Optical Engineering*, 60(2):020902, 2021.
6. Gerard A. Mourou, Toshiki Tajima, and Sergei V. Bulanov. Optics in the relativistic regime. *Rev. Mod. Phys.*, 78:309–371, Apr 2006.
7. P Zhang, SS Bulanov, D Seipt, AV Arefiev, and AGR Thomas. Relativistic plasma physics in supercritical fields. *Physics of Plasmas*, 27(5):050601, 2020.
8. A. Gonoskov, T. G. Blackburn, M. Marklund, and S. S. Bulanov. Charged particle motion and radiation in strong electromagnetic fields. *Rev. Mod. Phys.*, 94:045001, Oct 2022.
9. A. Fedotov, A. Ilderton, F. Karbstein, B. King, D. Seipt,

H. Taya, and G. Torgrimsson. Advances in qed with intense background fields. *Physics Reports*, 1010:1–138, 2023. Advances in QED with intense background fields.

10. Min Sup Hur, Bernhard Ersfeld, Hyojeong Lee, Hyunsuk Kim, Kyungmin Roh, Yunkyu Lee, Hyung Seon Song, Manoj Kumar, Samuel Yoffe, Dino A. Jaroszynski, and Hyyong Suk. Laser pulse compression by a density gradient plasma for exawatt to zettawatt lasers. *Nature Photonics*, 17(12):1074–1079, 2023.
11. V. M. Malkin, G. Shvets, and N. J. Fisch. Fast compression of laser beams to highly overcritical powers. *Phys. Rev. Lett.*, 82:4448–4451, May 1999.
12. Yuan Ping, Weifeng Cheng, Szymon Suckewer, Daniel S. Clark, and Nathaniel J. Fisch. Amplification of ultrashort laser pulses by a resonant raman scheme in a gas-jet plasma. *Phys. Rev. Lett.*, 92:175007, Apr 2004.
13. A. A. Andreev, C. Riconda, V. T. Tikhonchuk, and S. Weber. Short light pulse amplification and compression by stimulated Brillouin scattering in plasmas in the strong coupling regime. *Physics of Plasmas*, 13(5):053110, 05 2006.
14. Matthew R. Edwards, Qing Jia, Julia M. Mikhailova, and Nathaniel J. Fisch. Short-pulse amplification by strongly coupled stimulated Brillouin scattering. *Physics of Plasmas*, 23(8):083122, 08 2016.
15. Hui-Chun Wu, Zheng-Ming Sheng, and Jie Zhang. Chirped pulse compression in nonuniform plasma Bragg gratings. *Applied Physics Letters*, 87(20):201502, 11 2005.
16. J. P. Farmer, B. Ersfeld, and D. A. Jaroszynski. Raman amplification in plasma: Wavebreaking and heating effects. *Physics of Plasmas*, 17(11):113301, 11 2010.
17. P. Kaw, G. Schmidt, and T. Wilcox. Filamentation and trapping of electromagnetic radiation in plasmas. *The Physics of Fluids*, 16(9):1522–1525, 09 1973.
18. Matthew R. Edwards and Pierre Michel. Plasma transmission gratings for compression of high-intensity laser pulses. *Phys. Rev. Appl.*, 18:024026, Aug 2022.
19. G. Lehmann and K. H. Spatschek. Plasma-grating-based laser pulse compressor. *Phys. Rev. E*, 110:015209, Jul 2024.
20. R. F. Hubbard, B. Hafizi, A. Ting, D. Kaganovich, P. Sprangle, and A. Zigler. High intensity focusing of laser pulses using a short plasma channel lens. *Physics of Plasmas*, 9(4):1431–1442, 04 2002.
21. J. P. Palastro, D. Gordon, B. Hafizi, L. A. Johnson, J. Peñano, R. F. Hubbard, M. Helle, and D. Kaganovich. Plasma lenses for ultrashort multi-petawatt laser pulses. *Physics of Plasmas*, 22(12):123101, 12 2015.
22. D. Li, K. G. Miller, J. R. Pierce, W. B. Mori, A. G. R. Thomas, and J. P. Palastro. Spatiotemporal control of high-intensity laser pulses with a plasma lens. *Phys. Rev. Res.*, 6:013272, Mar 2024.
23. Y. Ma, J. A. Cardarelli, P. T. Campbell, S. Fourmaux, R. Fitzgarrald, M. D. Balcazar, A. F. Antoine, N. F. Beier, Q. Qian, A. E. Hussein, B. Kettle, S. R. Klein, K. Krushelnick, Y. F. Li, S. P. D. Mangles, G. Sarri, D. Seipt, V. Senthilkumaran, M. J. V. Streeter, L. Willingale, and A. G. R. Thomas. Single-shot diagnosis of electron energy evolution via streaked betatron x rays in a curved laser wakefield accelerator. *Phys. Rev. Lett.*, 132:225001, May 2024.
24. Y. Ma, D. Seipt, S. J. D. Dann, M. J. V. Streeter, C. A. J. Palmer, L. Willingale, and A. G. R. Thomas. Angular streaking of betatron x-rays in a transverse density gradient laser-wakefield accelerator. *Physics of Plasmas*, 25(11):113105, 11 2018.
25. M. Vargas, W. Schumaker, Z.-H. He, Z. Zhao, K. Behm, V. Chvykov, B. Hou, K. Krushelnick, A. Maksimchuk, V. Yanovsky, and A. G. R. Thomas. Improvements to laser wakefield accelerated electron beam stability, divergence, and energy spread using three-dimensional printed two-stage gas cell targets. *Applied Physics Letters*, 104(17):174103, 2014.
26. Jean-Claude Diels and Wolfgang Rudolph. *Ultrashort Laser Pulse Phenomena*. Academic Press, Burlington, 2 edition, 2006.
27. R. A. Fonseca, L. O. Silva, F. S. Tsung, V. K. Decyk, W. Lu, C. Ren, W. B. Mori, S. Deng, S. Lee, T. Katsouleas, and J. C. Adam. Osiris: A three-dimensional, fully relativistic particle in cell code for modeling plasma based accelerators. In Peter M. A. Sloot, Alfons G. Hoekstra, C. J. Kenneth Tan, and Jack J. Dongarra, editors, *Computational Science — ICCS 2002*, pages 342–351, Berlin, Heidelberg, 2002. Springer Berlin Heidelberg.
28. A. Davidson, A. Tableman, W. An, F. S. Tsung, W. Lu, J. Vieira, R. A. Fonseca, L. O. Silva, and W. B. Mori. Implementation of a hybrid particle code with a pic description in r–z and a gridless description in ϕ into osiris. *Journal of Computational Physics*, 281, 1 2015.
29. E. G. Gamaly, A. V. Rode, B. Luther-Davies, and V. T. Tikhonchuk. Ablation of solids by femtosecond lasers: Ablation mechanism and ablation thresholds for metals and dielectrics. *Physics of Plasmas*, 9(3):949–957, 03 2002.
30. B. C. Stuart, M. D. Feit, S. Herman, A. M. Rubenchik, B. W. Shore, and M. D. Perry. Optical ablation by high-power short-pulse lasers. *J. Opt. Soc. Am. B*, 13(2):459–468, Feb 1996.
31. Guo-Zheng Sun, Edward Ott, Y. C. Lee, and Parvez Guzdar. Self-focusing of short intense pulses in plasmas. *The Physics of Fluids*, 30(2):526–532, 02 1987.
32. J. Faure, V. Malka, J.-R. Marquès, P.-G. David, F. Amiranoff, K. Ta Phuoc, and A. Rousse. Effects of pulse duration on self-focusing of ultra-short lasers in

https://doi.org/10.1017/hpl.2025.18 Published online by Cambridge University Press

underdense plasmas. *Physics of Plasmas*, 9(3):756–759, 03 2002.

33. P. Polynkin and M. Kolesik. Critical power for self-focusing in the case of ultrashort laser pulses. *Phys. Rev. A*, 87:053829, May 2013.
34. Yanqing Deng, Dongning Yue, Mufei Luo, Xu Zhao, Yaojun Li, Xulei Ge, Feng Liu, Suming Weng, Min Chen, Xiaohui Yuan, and et al. Effects of second-order dispersion of ultrashort laser pulse on stimulated raman scattering. *High Power Laser Science and Engineering*, 10:e39, 2022.
35. Evan S. Dodd and Donald Umstadter. Coherent control of stimulated Raman scattering using chirped laser pulses. *Physics of Plasmas*, 8(8):3531–3534, 08 2001.
36. S. C. Wilks, W. L. Kruer, E. A. Williams, P. Amendt, and D. C. Eder. Stimulated Raman backscatter in ultraintense, short pulse laser–plasma interactions. *Physics of Plasmas*, 2(1):274–279, 01 1995.

https://doi.org/10.1017/hpl.2025.18 Published online by Cambridge University Press